Article

Enhanced Ion Conduction in $Li_{2.5}Zn_{0.25}PS_4$ via Anion Doping

Xuyong Feng, Po-Hsiu Chien, Sawankumar Patel, Yan Wang, and Yan-Yan Hu*

Read Online

ACCESS | Metrics & More | Article Recommendations | Supporting Information

ABSTRACT: $Li_{1+2x}Zn_{1-x}PS_4$ was computationally predicted to have superionic conductivity of over 50 mS/cm. However, experimental efforts so far have only yielded ionic conductivities on the order of 10^{-4} S/cm, due to difficulty in producing phase-pure crystalline products. Here, to improve phase purity and enhance ionic conductivity, Cl- doping is employed to synthesize $Li_{1+2x-y}Zn_{1-x}PS_{4-y}Cl_y$, which is shown to stabilize $Li_{1+2x}Zn_{1-x}PS_4$ from decomposing to Li_3PS_4. $Li_{2.5}Zn_{0.25}PS_4$ which shows the highest ionic conductivity among the $Li_{1+2x}Zn_{1-x}PS_4$ samples is chosen as an example to study. After incorporating only a small amount of Cl, the ionic conductivity increases from 0.6 mS/cm for $Li_{2.5}Zn_{0.25}PS_4$ to 3.5 mS/cm for $Li_{2.4}Zn_{0.25}PS_{3.9}Cl_{0.1}$ at 25 °C. In addition, the activation energy is reduced from 0.33 to 0.27 eV. The phase purity and fine structure of $Li_{1+2x-y}Zn_{1-x}PS_{4-y}Cl_y$ are determined with XRD, and ^7Li, ^{31}P, ^{35}Cl solid-state NMR characterizations. The experimental data confirm the success of Cl^- doping. In addition, $Li_{2.4}Zn_{0.25}PS_{3.9}Cl_{0.1}$ exhibits a low electronic conductivity of 1.21×10^{-9} S/cm and a wide electrochemical stability window.
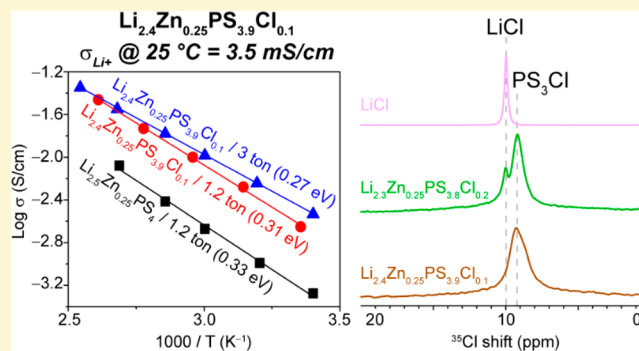
INTRODUCTION

All-solid-state batteries are promising to offer enhanced safety and energy density.[1−3] Developing highly conductive solid electrolytes is essential to high performance all-solid-state batteries, especially for high-power applications. Researchers continue to search for new types of solid electrolytes with high ionic conductivities and stability.[4,5] Wang et al. discovered the body-centered cubic feature in several superionic sulfide conductors and used it as a screening descriptor for potential new ionic conductors.[3] Following this work, Richards et al. investigated a sulfide material $LiZnPS_4$ with a body-centered cubic sublattice with density functional theory (DFT) and ab initio molecular dynamics (AIMD).[5] Taking both thermal stability and ionic conductivity into account, the optimized composition is $Li_{2.5}Zn_{0.25}PS_4$, in which excess Li^+ partially replaces Zn^{2+}. It is predicted to have a high ionic conductivity of more than 50 mS/cm and a low activation energy of 0.14 eV.

Recently, experimental efforts have been made to prepare $Li_{1+2x}Zn_{1-x}PS_4$, aiming to achieve the predicted ionic conductivity. To prepare $Li_{1+2x}Zn_{1-x}PS_4$ via solid state reaction, nanosized ZnS is needed to improve the reactivity at relatively low temperature.[6] Impurities were found within all the $Li_{1+2x}Zn_{1-x}PS_4$ samples, such as $Li_4P_2S_6$ with small x values and Li_3PS_4 with large x values. The impurities led to much lower conductivity than the computed value. The highest ionic conductivity obtained from reported experiments is only 0.84 mS/cm with x = 0.75 ($Li_{2.5}Zn_{0.25}PS_4$). Naoki et al. also prepared $Li_{1+2x}Zn_{1-x}PS_4$ from $LiZnPS_4$ and Li_3PS_4, in order to

suppress the evaporation of S and thus formation of $Li_4P_2S_6$ impurity.[7] But crystallinity decreases with increasing x, and the highest ionic conductivity achieved is 0.57 mS/cm at x = 0.625 ($Li_{2.25}Zn_{0.375}PS_4$).

In order to prepare highly conductive $Li_{1+2x}Zn_{1-x}PS_4$, phase pure crystalline products with large x values are needed. In addition, Cl^- doping in the S^{2-} sites is shown as a good strategy to enhance ionic conductivity of sulfide-based electrolytes. Kanno et al. reported a Cl^- doped $Li_{9.54}Si_{1.74}P_{1.44}S_{11.7}Cl_{0.3}$, which delivers a high ionic conductivity of 25 mS/cm at room temperature.[8] Cl^- was also introduced to tetragonal Na_3PS_4, which has significantly enhanced the ionic conductivity.[9,10] Here, we introduce a small amount of LiCl to partially replace Li_2S as one precursor, which is shown to suppress the formation of Li_3PS_4 and enhance crystallinity. The optimized conductivity reaches 3.5 mS/cm for $Li_{2.4}Zn_{0.25}PS_{3.9}Cl_{0.1}$, which is about 4 times the values reported for $Li_{2.5}Zn_{0.25}PS_4$.[6] $Li_{2.4}Zn_{0.25}PS_{3.9}Cl_{0.1}$ also exhibits significantly enhanced stability with a low electronic conductivity and a large electrochemical stability window.

■ EXPERIMENTAL SECTION

ZnS nanoparticles were prepared by a precipitation method using $Zn(CH_3COO)_2$ and Na_2S as the source of Zn and S.[11] Li_2S, P_2S_5, and LiCl were purchased from Sigma-Aldrich and LiCl was dried under dynamic vacuum at 200 °C for 12 h before use. Li_2S, nanosized ZnS, P_2S_5, and LiCl were mixed with a Li:P:S:Cl molar ratio of $(1 + 2x − y):(1 − x):(4 − y):y$ and manually ground for 10 min. The premixed powders were then placed in a ZrO_2 jar (two ZrO_2 balls; 10 mm) and ball-milled (Spex 8000M) for 20 h under vacuum. After ball-milling, the mixed powders were pelletized into a disk (6 mm in diameter and 1 mm in thickness) and sintered at 260 °C for 12 h under Ar. All operations were performed under the protection of Ar gas in a glovebox (Mbraun, H_2O < 0.5 ppm, O_2 < 0.5 ppm).

Powder XRD experiments were performed using a Philips X'Pert powder diffractometer at 45 kV and 40 mA with Cu Kα radiation (λ = 1.5406 Å). The as-synthesized pellets were ground gently into fine powders for a short time and then placed on a zero-background holder, which was sealed with a Kapton film to avoid air exposure. The patterns were collected at room temperature with a 2θ range from 10° to 80° and a scan rate of 2°/min.

^{6}Li, ^{7}Li, and ^{31}P magic-angle-spinning (MAS) NMR experiments were performed on a Bruker Avance-III 500 spectrometer at the Larmor frequency of 73.6, 194.4, and 202.4 MHz, respectively. A spinning rate of 25 kHz was used for all the experiments. A single pulse sequence was employed to acquire all ^{6}Li and ^{7}Li NMR spectra with a solid 90° pulse length and a recycle delay of 4.75 μs and 500 s and 3.35 μs and 5 s for ^{6}Li and ^{7}Li NMR, respectively. ^{31}P NMR was recorded with a rotor-synchronized spin−echo sequence with a 90° pulse length of 4.2 μs and a recycle delay of 200 s. ^{6,7}Li and ^{31}P NMR spectra were calibrated to $LiCl_{(s)}$ at −1.1 ppm[12] and 85% $H_3PO_{4(l)}$ at 0 ppm, respectively. ^{35}Cl MAS NMR experiments were performed on a Bruker 830 spectrometer using a home-built 3.2 mm probe[13] at the Larmor frequency of 81.3 MHz. The rotor-synchronized spin−echo sequence with a solid 90° pulse length of 2.9 μs and a recycle delay of 20 s was employed. ^{35}Cl NMR spectra were calibrated to $LiCl_{(s)}$ at 9.93 ppm.

Variable-temperature (VT) solid-state ^{7}Li MAS NMR experiments were carried out on a Bruker Avance III spectrometer (11.75 T) with a ^{7}Li Larmor frequency at 194.319 MHz and a spinning rate of 5 kHz. VT ^{7}Li MAS NMR spectra of $Li_{2.4}Zn_{0.25}PS_{3.9}Cl_{0.1}$ were acquired using the Bruker Laser probe[14] from 25 to 300 °C. The temperature was calibrated with the ^{79}Br NMR shift of KBr.[15] After adjusting the temperature to the desired value before each acquisition, 5 min (during heating) or 15 min (during cooling) was allowed to reach thermal equilibration. One-dimensional ^{7}Li MAS NMR spectra were collected by a 90° single-pulse excitation of 3.15 μs and with a recycle delay of 5 s. Sixteen scans were accumulated for each spectrum. After each acquisition of a 1D ^{7}Li MAS NMR spectrum, ^{7}Li longitudinal NMR relaxation time (T_1) was measured with an inversion−recovery pulse sequence. ^{7}Li chemical shift was referenced to 1 M $LiCl_{(l)}$ at 0 ppm. All the analyses of NMR spectra and ^{7}Li T_1 times were performed on Bruker Topspin v.4.0.3.

The ionic conductivity of $Li_{2.5−y}Zn_{0.25}PS_{4−y}Cl_y$ was measured at 25 °C using Ac electrochemical impedance spectroscopy (EIS) in the frequency range from 5 MHz to 1 Hz with a potential of 50 mV. To extract the activation energy of ion conduction in $Li_{2.5−y}Zn_{0.25}PS_{4−y}Cl_y$, variable-temperature impedance measurements were then performed from room temperature to 120 °C in a CSZ microclimate chamber. The as-synthesized $Li_{2.5−y}Zn_{0.25}PS_{4−y}Cl_y$ disks were sandwiched by indium foils (4.7 mm in diameter) and sealed in a home-built cylindrical cell[16] for all measurements. The electronic conductivity of $Li_{2.5−y}Zn_{0.25}PS_{4−y}Cl_y$ was measured by applying a voltage of 3 V on In|$Li_{2.5−y}Zn_{0.25}PS_{4−y}Cl_y$|In and measuring current until it becomes stable. Cyclic voltammetry measurements were carried out on Li|$Li_{2.4}Zn_{0.25}PS_{3.9}Cl_{0.1}$|Stainess steel between −0.3 and 5 V at a scanning rate of 10 mV/s.

■ RESULTS AND DISCUSSION

The space group of pristine $LiZnPS_4$ is $I\bar{4}$, with Li^+ fully occupying 2a sites and Zn^{2+} fully occupying 2b sites. After partly replacing Zn^{2+} with Li^+ ($Li_{1+2x}Zn_{1−x}PS_4$), the 2b sites are shared by Li^+ and Zn^{2+}, and extra Li^+ occupies 2d sites (Figure 1a). Previous work[6] has shown that Li_3PS_4 and Li_2PS_3 are two
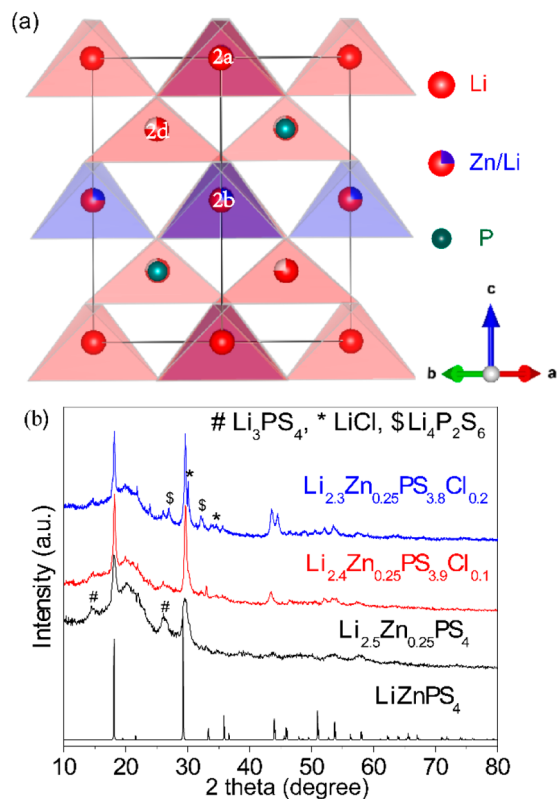

Figure 1. (a) Crystal structure of $Li_{2.5}Zn_{0.25}PS_4$, (b) XRD patterns of $Li_{2.5−y}Zn_{0.25}PS_{4−y}Cl_y$ (y = 0, 0.1, 0.2); the standard XRD pattern of $LiZnPS_4$ is shown as a reference.

observed impurities accompanying the synthesis of $Li_{1+2x}Zn_{1−x}PS_4$. This work suggests when $x \leq 0.5$, the main impurity is $Li_4P_2S_6$ (Figure S1a), with P^{5+} partially reduced to P^{4+}. When the x value increases to 0.75 ($Li_{2.5}Zn_{0.25}PS_4$), $Li_4P_2S_6$ almost disappears and Li_3PS_4 emerges as the main impurity phase. This is consistent with computational studies reporting that when the amount of Zn reduces, more Li occupies the 2b and 2d sites.[5] The structure becomes unstable and is likely to decompose to Li_3PS_4 and $Li_{1+2x−2\delta}Zn_{1−x+\delta}PS_4$. Another change with higher x values is the peak intensity decreases in the XRD pattern, which infers lower crystallinity. The conductivity of $Li_{1+2x}Zn_{1−x}PS_4$ is maximized at x = 0.75 ($Li_{2.5}Zn_{0.25}PS_4$) (Figure 2), which is about 0.6 mS/cm at 25 °C (Figure S1b), which agrees very well with previous findings.[6,7]

To further improve the ionic conductivity of $Li_{2.5}Zn_{0.25}PS_4$, anion-doping with $Cl^−$ is employed. $Cl^−$ replacement of $S^{2−}$ will lead to slight Li deficiency, structural distortion, and changes in Li^+−host interactions. Therefore, $Cl^− \rightarrow S^{2−}$ exchange will affect the stability of the resulting structure and impact Li^+ transport. As shown in Figure 1b, the amount of Li_3PS_4 impurity is greatly reduced and the crystallinity is significantly enhanced after $Cl^−$ doping in $Li_{2.4}Zn_{0.25}PS_{3.9}Cl_{0.1}$. However, the amount of Cl dopant is limited due to the stable $PS_4^{3−}$. When y increases to 0.2 in $Li_{2.5−y}Zn_{0.25}PS_{4−y}Cl_y$, not all
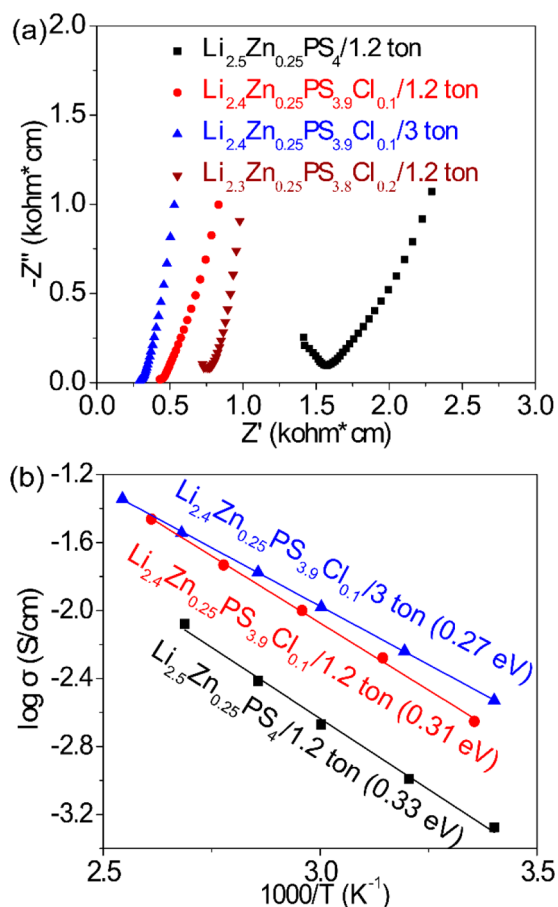
Figure 2. AC impedance spectra (a) and Arrhenius plots (b) of $Li_{2.5-y}Zn_{0.25}PS_{4-y}Cl_y$ ($y = 0, 0.1, 0.2$) samples with varied Cl^- content and prepared under a pressure of 1.2 tons or 3 tons.

Figure 3. (a) DC polarization curves of $Li_{2.5}Zn_{0.25}PS_4$ and $Li_{2.4}Zn_{0.25}PS_{3.9}Cl_{0.1}$ under 3 V (diameter of In current collector is 4.7 mm, thickness is 1 mm), and (b) cyclic voltammogram for the $Li_{2.4}Zn_{0.25}PS_{3.9}Cl_{0.1}$ (SS represents stainless steel).

Cl^- can be incorporated into $Li_{2.5}Zn_{0.25}PS_4$, and the remaining LiCl exists as an impurity ($Li_{2.3}Zn_{0.25}PS_{3.8}Cl_{0.2}$). In addition, with $y > 0.1$, the impurity of Li_2PS_3 forms after sintering, which will further lower the ionic conductivity.

With enhanced phase purity and crystallinity after Cl^- doping ($Li_{2.5-y}Zn_{0.25}PS_{4-y}Cl_y$), the conductivity also exhibited significant improvement (Figure 2). When $y = 0.1$ in $Li_{2.5-y}Zn_{0.25}PS_{4-y}Cl_y$, the conductivity increases to about 2.2 mS/cm at 25 °C ($Li_{2.4}Zn_{0.25}PS_{3.9}Cl_{0.1}$/1.2 ton) and further improves to be 3.5 mS/cm with higher pressure ($Li_{2.4}Zn_{0.25}PS_{3.9}Cl_{0.1}$/3 ton). Beyond $y = 0.1$, the ionic conductivity decreases due to the increased formation of impurities with low ionic conductivities including $Li_4P_2S_6$. Besides improvement in the ionic conductivity, activation energy is also reduced with Cl doping. The activation energy of $Li_{2.5}Zn_{0.25}PS_4$ is about 0.33 eV, which decreases to 0.31 eV in $Li_{2.4}Zn_{0.25}PS_{3.9}Cl_{0.1}$ and further decreases to 0.27 eV with higher pressure ($Li_{2.4}Zn_{0.25}PS_{3.9}Cl_{0.1}$/3 ton). The enhanced total ionic conductivity and decreased activation energy with relatively high pressure are due to reduced grain boundary resistance for ion transport.[17,18]

In addition to high ionic conductivity, low electronic conductivity is also important for solid electrolytes, in order to minimize self-discharge, enhance stability, and reduce dendritic lithium formation.[19] The DC polarization curves of $Li_{2.5}Zn_{0.25}PS_4$ and $Li_{2.4}Zn_{0.25}PS_{3.9}Cl_{0.1}$ under an applied voltage of 3 V are shown in Figure 3a, based on which the electronic conductivities of $Li_{2.5}Zn_{0.25}PS_4$ and $Li_{2.4}Zn_{0.25}PS_{3.9}Cl_{0.1}$ are

calculated to be 1.35×10^{-9} S/cm and 1.21×10^{-9} S/cm, respectively, much lower than the electronic conductivity of widely studied solid-state electrolyte material $Li_7La_3Zr_2O_{12}$.[19]

To evaluate the electrochemical stability, the cyclic voltammogram of the $Li_{2.4}Zn_{0.25}PS_{3.9}Cl_{0.1}$ is measured and shown in Figure 3b. The open circuit voltage of Li/$Li_{2.4}Zn_{0.25}PS_{3.9}Cl_{0.1}$/Stainless steel is ~2 V, and the cell is first discharged to −0.3 V vs Li/Li⁺. During reduction, only one process happens at about −0.2 V (vs Li/Li⁺), which is the plating of Li on stainless steel. According to previous reports, decomposition of $Li_{2.25}Zn_{0.375}PS_4$ to form Li_2S, Zn_3P_2, and ZnP_2 happens when the potential is less than 1 V vsLi/Li⁺.[7] Further reactions leading to the formation of electronically conductive Zn and/or Li−Zn alloy, which allows non-self-limiting SEI formation at the Li-LZPS interface or other parasitic reactions in the bulk electrolyte, compromising the electrochemical stability of LZPS.[7,16] Lower Zn^{2+} content in $Li_{1+2x}Zn_{1-x}PS_4$ is expected to eventually help reduce the total electronic conductivity of the SEI layer between $Li_{1+2x}Zn_{1-x}PS_4$. Here, no obvious decomposition peak is detected during the discharge process, which suggests improved stability of $Li_{2.4}Zn_{0.25}PS_{3.9}Cl_{0.1}$ against Li metal. The improved stability against Li metal is due to the lower electronic conductivity after Cl doping and reduced Zn amount compared to $Li_{2.25}Zn_{0.375}PS_4$. During the charge process, Li stripping occurs at about 0.2 V and no apparent oxidations are observed up to 5 V (vs Li/Li⁺), indicating good

electrochemical stability of $Li_{2.4}Zn_{0.25}PS_{3.9}Cl_{0.1}$ at high voltages, which makes it compatible with most commercial cathodes.

To probe the local structure and Li^+ mobility, solid-state NMR is employed (Figure 4−7). The ^6Li NMR spectrum of
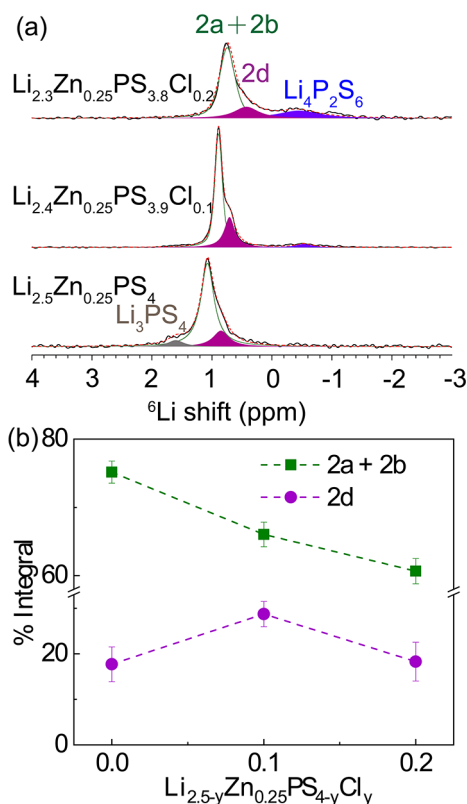

Figure 4. ^6Li NMR spectra of $Li_{2.5-y}Zn_{0.25}PS_{4-y}Cl_y$ (y = 0, 0.1, 0.2) samples (a), and the quantification results of different Li sites (b).

$Li_{2.5}Zn_{0.25}PS_4$ exhibits two main peaks at around 0.9 and 1.2 ppm, respectively. Based on the structure of $Li_{1+2x}Zn_{1-x}PS_4$, the difference in 2a, 2b, and 2d Li sites is very small and only manifests in the second coordination shell: 2a+2b is surrounded by Li^+ and P^{5+} while 2d is surrounded by Li^+ and Zn^{2+}. The 2a+2b ^6Li NMR resonance is expected to appear at lower field (higher ppm values) based on electron charge distribution compared with the 2d ^6Li resonance. Therefore, the 0.9-ppm ^6Li resonance is assigned to Li at 2d sites while the 1.2-ppm resonance is assigned to Li at 2a and 2b sites. The area integrals of the Li NMR resonances are proportional to the actual Li occupancies at different structural sites, which are used to perform quantitative site occupancy analysis. Detailed site fractions based on spectra analysis are shown in Figure 4b. For an ideal $Li_{1+2x}Zn_{1-x}PS_4$, the fraction of Li^+ at 2d site should be within the range of $[x/(1 + 2x), 1/(1 + 2x)]$, i.e., [30%, 40%] for $Li_{2.5}Zn_{0.25}PS_4$, calculated based on two extreme cases, 2a+2b fully occupied or 2d fully occupied. But according to ^6Li NMR, the Li_{2d} fraction is only around 20%, which means the real composition is not $Li_{2.5}Zn_{0.25}PS_4$ but $Li_{2.5-2\delta}Zn_{0.25+\delta}PS_4$ with a lower predicted ionic conductivity.[5] A similar phenomenon has been observed with neutron diffraction.[6] The Li_{2d} fraction increases to about 30% in $Li_{2.4}Zn_{0.25}PS_{3.9}Cl_{0.1}$, which is close to the theoretical ratio and suggests higher purity. In addition, Li_3PS_4 almost disappears and thus further confirms the minimization of Li_3PS_4 formation with Cl doping. However, a small amount of

$Li_4P_2S_6$ appears, especially in $Li_{2.3}Zn_{0.25}PS_{3.8}Cl_{0.2}$, which agrees with the XRD results.

Furthermore, variable-temperature ^7Li solid state NMR is used to study the Li^+ mobility and thermal stability of $Li_{2.4}Zn_{0.25}PS_{3.9}Cl_{0.1}$ (Figure 5 and 6). Figure 5 summarizes one-

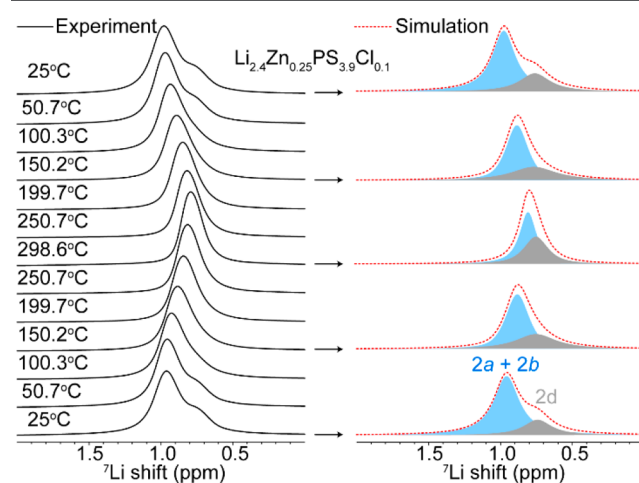**Figure 5.** Variable-temperature ^7Li NMR spectra of $Li_{2.4}Zn_{0.25}PS_{3.9}Cl_{0.1}$ acquired at a MAS rate of 5 kHz. Selected spectral simulations are shown on the right.

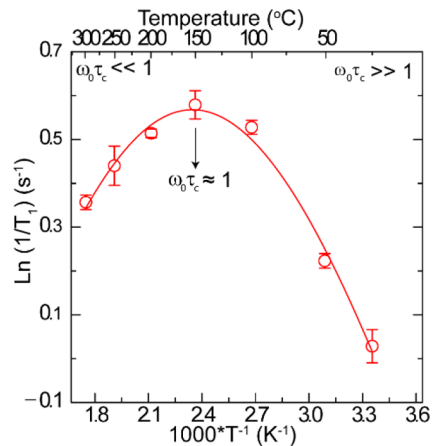**Figure 6.** Variable-temperature ^7Li T_1 NMR relaxation time measurements of $Li_{2.4}Zn_{0.25}PS_{3.9}Cl_{0.1}$. The solid line represents the fit using the BPP expression.[18]

dimensional ^7Li MAS NMR spectra of $Li_{2.4}Zn_{0.25}PS_{3.9}Cl_{0.1}$ acquired within the temperature range from 25 °C to 298.6 °C. Selective spectral analyses are presented in the right panel of Figure 5. At room temperature, the Li fraction at 2d sites (Figure 5, right panel) adds up to 30%, which leaves 70% of lithium to collectively distribute among 2a and 2b sites; this result is in line with ^6Li MAS (25 kHz) NMR (Figure 4). Upon heating $Li_{2.4}Zn_{0.25}PS_{3.9}Cl_{0.1}$, a characteristic feature that signifies chemical exchange between Li^+ at different sites (2a + 2b vs 2d) is identified. The ^7Li signals (2a + 2b and 2d) migrate toward each other with increasing temperature and nearly coalesce as a single peak resonating at the center-of-mass with respect to the two signals (2a + 2b and 2d) at 298.6 °C.

Upon cooling, Li^+ kinetics slows down and the merged ^7Li peaks split into two partially resolved resonances at room

temperature as was identified before heating (Figure 5), suggesting good thermal stability under 300 °C.

Li ion dynamics are further investigated with variable-temperature ^7Li T_1 NMR relaxation time measurements. As shown in Figure 6, the dependence of NMR relaxation rates (i.e., $R_1 = 1/T_1$ in Hz) on temperatures presents a so-called "NMR rate peak", which is induced by a Li^+ diffusional process.[18] The rate maximum appears at ~150 °C, at which the Li^+ jump rate can be estimated with $\omega_0\tau_c \approx 1$. Since ^7Li T_1 measurements are performed with a ^7Li Larmor frequency $\omega_0/2\pi = 194.319$ MHz, τ_c is calculated as 8.2×10^{-10} s at 150 °C. If we assume the jump distance, a, between $2a/2b$ and $2d$ (3.69 Å) remains unvaried at 150 °C, we obtain a diffusion coefficient $= 2.8 \times 10^{-7}$ cm^2 s^{-1} through the Einstein–Smoluchowski equation, $D = a^2/(6\tau_c)$ (3D diffusion[5]). This diffusivity extracted from ^7Li T_1 measurements is lower than the computed value on this material (~6×10^{-6} cm^2 s^{-1}).[5] In addition, fitting the diffusion-induced ^7Li rate peak (Figure 6) using the BPP model[20] yields an activation energy (E_{HT}) of only 0.13 eV (Table S1), which is close to the computational results (0.14 eV) but significantly lower than that of 0.27 eV probed by EIS.[5] NMR T_1 relaxation rate is typically sensitive to ion dynamics on a time scale that is much shorter than what impedance accesses;[21] thus, higher activation energy revealed by EIS most likely relates to macroscopic diffusion while NMR T_1 relaxation sheds light on microscopic diffusion and/or localized ion dynamics. As a result, the low activation energy obtained from the high-T flank ($\omega_0\tau_c \ll 1$) of the ^7Li rate peak (Figure 6) is associated with local ion movement. It is worth noting that in order to enable a 3D diffusion in $Li_{2.4}Zn_{0.25}PS_{3.9}Cl_{0.1}$, successful hopping from $2a$ sites to $2b$ sites is necessary and this diffusion process should be treated as a rate-determining step of the overall ion conduction.

Lastly, our BPP fitting (see eqs 1 and 2) results in a β value of 1.76 for the "asymmetric" ^7Li rate peak.

$$R_1(\omega) = C\left[\frac{\tau_c}{1 + (\omega_0\tau_c)^\beta} + \frac{4\tau_c}{1 + (2\omega_0\tau_c)^\beta}\right] \quad (1)$$

$$\tau_c^{-1} = \tau_{c,0}^{-1}\exp(-Ea/k_bT) \quad (2)$$

$R_1 = 1/T_1 = $ relaxation rate (^7Li)
$C = $ constant
$\tau_c = $ correlation time
$\tau_{c,0} = $ pre-factor
$\omega_0 = $ Larmor frequency (^7Li)
β ($1 < \beta \leq 2$) = an exponent to specify the frequency dependence of the rate peak on both the low-T and high-T side.[20,22]

A β value of 2 is in general found with uncorrelated 3D motion as was originally demonstrated in the case of liquid.[23] However, solid electrolytes with structural disorder often show a β value < 2,[24,25] which suggests a strong correlation effect[26] induced by Coulomb interactions.[27] Therefore, a β value of 1.76 for $Li_{2.4}Zn_{0.25}PS_{3.9}Cl_{0.1}$ indicates a correlated 3D Li^+ motion, in which the Li^+ dynamics are affected by correlation effects originating from structural disorder and the $Li^+–Li^+$, $Li^+–S^{2-}$, and $Li^+–Cl^-$ interactions. Incorporation of halogens into PS_4^{3-} anionic sublattice has been shown to effectively perturb their interactions with positively charged mobile carriers such as Li^+/Na^+.[10,28] In $Li_{2.4}Zn_{0.25}PS_{3.9}Cl_{0.1}$, we expect to observe such correlation effects due to the formation of PS_3Cl^{2-}, and the broken symmetry in PS_4^{3-} anionic sublattice

may indirectly facilitate Li-ion conduction by softening the Li–S interactions.[29]

In addition to $^{6,7}Li$ NMR, ^{31}P and ^{35}Cl NMR spectra are also acquired and shown in Figure 7. $Li_{2.5}Zn_{0.25}PS_4$ only has

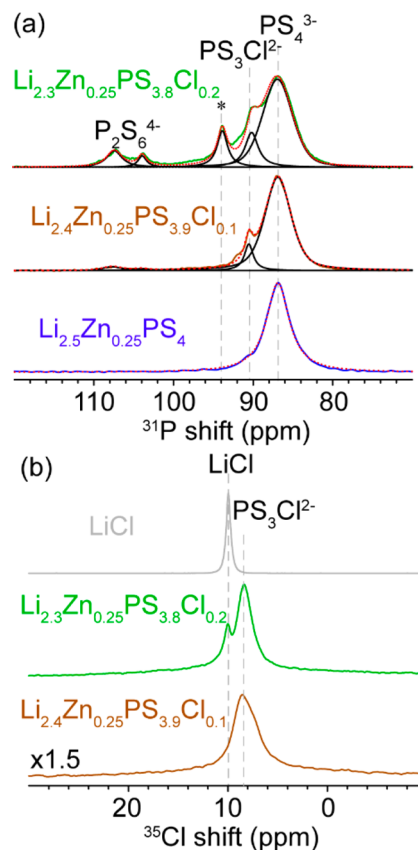**Figure 7.** ^{31}P (a) and ^{35}Cl (b) NMR spectra of different $Li_{2.5-y}Zn_{0.25}PS_{4-y}Cl_y$ samples ($y = 0, 0.1, 0.2$); * denotes an unknown impurity. Dotted red lines in (a) are simulated spectra.

one broad peak at around 87 ppm, which is from the PS_4 framework. After doping with Cl, S is partially replaced by Cl and then a fraction of the PS_4 framework changes to PS_3Cl, which shifts the ^{31}P resonance to the left. Another two peaks at 103 ppm and 106 ppm appear with Cl doping, which are from the impurity of Li_4PS_6.[10,30] In $Li_{2.3}Zn_{0.25}PS_{3.8}Cl_{0.2}$, more impurities form, suggested by the extra peak at 93 ppm. For $Li_{2.4}Zn_{0.25}PS_{3.9}Cl_{0.1}$, the amount of Li_4PS_6 is small. The ratio of PS_3Cl is about 10%, confirming 0.1 Cl doped into the $Li_{2.4}Zn_{0.25}PS_{3.9}Cl_{0.1}$ successfully. ^{35}Cl NMR spectra of $Li_{2.4}Zn_{0.25}PS_{3.9}Cl_{0.1}$ only have one peak, which is from Cl in $Li_{2.4}Zn_{0.25}PS_{3.9}Cl_{0.1}$. The amount of Cl in the nominal $Li_{2.3}Zn_{0.25}PS_{3.8}Cl_{0.2}$ is calculated to be about 0.14 based on the ^{35}Cl NMR, and the remaining Cl exists as LiCl impurity (Figure 7b). The ^{31}P and ^{35}Cl NMR proves the success of Cl doping and the maximum y value in $Li_{2.5-y}Zn_{0.25}PS_{4-y}Cl_y$ is determined to be 0.14.

■ CONCLUSION

In summary, we have successfully replaced a small amount of S^{2-} in $Li_{2.5}Zn_{0.25}PS_4$ with Cl^-, which enhances the ionic conductivity by 4-fold to about 3.5 mS/cm at room temperature. Our investigation reveals three reasons why Cl^- doping enhances the ionic conductivity: (1) improved phase

purity, (2) enhanced crystallinity of $Li_{2.4}Zn_{0.25}PS_{3.9}Cl_{0.1}$, and (3) lowered electrostatic attraction between Li^+ and the anion framework. For Li-rich $Li_{1+2x}Zn_{1-x}PS_4$ with high x ($x > 0.75$), it tends to decompose to Li_3PS_4 at high temperature; therefore, low temperature or Li deficiency helps stabilize $Li_{1+2x}Zn_{1-x}PS_4$. With a small amount of Cl doping in $Li_{2.5}Zn_{0.25}PS_4$, the Li^+ amount decreases, the impurity of Li_3PS_4 is observed to decrease, and the crystallinity is enhanced. ^{31}P NMR and ^{35}Cl NMR prove the successful doping of Cl into the structure of $Li_{2.4}Zn_{0.25}PS_{3.9}Cl_{0.1}$, and the maximum y value in $Li_{2.5-y}Zn_{0.25}PS_{4-y}Cl_y$ is determined to be between 0.1 and 0.2. The electrochemical stability of $Li_{2.4}Zn_{0.25}PS_{3.9}Cl_{0.1}$ is evaluated with cyclic voltammetry, which shows improved stability compared to $Li_{2.25}Zn_{0.375}PS_4$, due to the reduced content of Zn and decrease in electronic conductivity.

■ ASSOCIATED CONTENT

ⓢ Supporting Information

The Supporting Information is available free of charge at https://pubs.acs.org/doi/10.1021/acs.chemmater.0c00025.

> XRD patterns and AC impedance of $Li_{1+2x}Zn_{1-x}PS_4$ (x = 0.5, 0.75, 0.85), variable-temperature AC impedance of $Li_{2.5-y}Zn_{0.25}PS_{4-y}Cl_y$ (y = 0, 0.1).

■ AUTHOR INFORMATION

Corresponding Author

Yan-Yan Hu — *Department of Chemistry and Biochemistry, Florida State University, Tallahassee, Florida 32306, United States; Center of Interdisciplinary Magnetic Resonance, National High Magnetic Field Laboratory, Tallahassee, Florida 32310, United States;* ⓞ orcid.org/0000-0003-0677-5897; Email: yhu@fsu.edu

Authors

Xuyong Feng — *Department of Chemistry and Biochemistry, Florida State University, Tallahassee, Florida 32306, United States*

Po-Hsiu Chien — *Department of Chemistry and Biochemistry, Florida State University, Tallahassee, Florida 32306, United States; Center of Interdisciplinary Magnetic Resonance, National High Magnetic Field Laboratory, Tallahassee, Florida 32310, United States*

Sawankumar Patel — *Department of Chemistry and Biochemistry, Florida State University, Tallahassee, Florida 32306, United States*

Yan Wang — *Advanced Materials Lab, Samsung Research America, Burlington, Massachusetts 01803, United States*

Complete contact information is available at:
https://pubs.acs.org/10.1021/acs.chemmater.0c00025

Notes

The authors declare no competing financial interest.

■ ACKNOWLEDGMENTS

■ REFERENCES

(1) Du, M. Recent Advances in the Interface Engineering of Solid-State Li-Ion Batteries with Artificial Buffer Layers: Challenges, Materials, Construction, and Characterization. *Energy Environ. Sci.* **2019**, *12*, 1780−1804.

(2) Liang, J. Recent Progress on Solid-State Hybrid Electrolytes for Solid-State Lithium Batteries. *Energy Stor. Mater.* **2019**, *21*, 308−334.

(3) Wang, Y.; Richards, W. D.; Ong, S. P.; Miara, L. J.; Kim, J. C.; Mo, Y.; Ceder, G. Design Principles for Solid-State Lithium Superionic Conductors. *Nat. Mater.* **2015**, *14* (10), 1026−1031.

(4) Zhu, Z.; Chu, I.-H.; Ong, S. P. $Li_3Y(PS_4)_2$ and $Li_5PS_4Cl_2$: New Lithium Superionic Conductors Predicted from Silver Thiophosphates Using Efficiently Tiered Ab Initio Molecular Dynamics Simulations. *Chem. Mater.* **2017**, *29*, 2474−2484.

(5) Richards, W. D.; Wang, Y.; Miara, L. J.; Kim, J. C.; Ceder, G. Design of $Li_{1+2x}Zn_{1-x}PS_4$, a New Lithium Ion Conductor. *Energy Environ. Sci.* **2016**, *9* (10), 3272−3278.

(6) Kaup, K.; Lalere, F.; Huq, A.; Shyamsunder, A.; Adermann, T.; Hartmann, P.; Nazar, L. F. Correlation of Structure and Fast Ion Conductivity in the Solid Solution Series $Li_{1+2x}Zn_{1-x}PS_4$. *Chem. Mater.* **2018**, *30*, 592−596.

(7) Suzuki, N.; Richards, W. D.; Wang, Y.; Miara, L. J.; Kim, J. C.; Jung, I.-S.; Tsujimura, T.; Ceder, G. Synthesis and Electrochemical Properties of I4̄-Type $Li_{1+2x}Zn_{1-x}PS_4$ Solid Electrolyte. *Chem. Mater.* **2018**, *30*, 2236−2244.

(8) Kato, Y.; Hori, S.; Saito, T.; Suzuki, K.; Hirayama, M.; Mitsui, A.; Yonemura, M.; Iba, H.; Kanno, R. High-Power All-Solid-State Batteries Using Sulfide Superionic Conductors. *Nature Energy* **2016**, *1* (4), 16030.

(9) Chu, I.-H.; Kompella, C. S.; Nguyen, H.; Zhu, Z.; Hy, S.; Deng, Z.; Meng, Y. S.; Ong, S. P. Room-Temperature All-Solid-State Rechargeable Sodium-Ion Batteries with a Cl-Doped Na_3PS_4 Superionic Conductor. *Sci. Rep.* **2016**, *6* (1), 33733.

(10) Feng, X.; Chien, P.-H.; Zhu, Z.; Chu, I.-H.; Wang, P.; Immediato-Scuotto, M.; Arabzadeh, H.; Ong, S. P.; Hu, Y.-Y. Studies of Functional Defects for Fast Na-Ion Conduction in $Na_{3-y}PS_{4-x}Cl_x$ with a Combined Experimental and Computational Approach. *Adv. Funct. Mater.* **2019**, *29* (9), 1807951.

(11) Phoohinkong, W.; Sukonket, T. A Simple Method for Large-Scale Synthesis of Nano-Sized Zinc Sulfide. *Adv. Mater. Res.* **2014**, *979*, 188−191.

(12) Meyer, B. M.; Leifer, N.; Sakamoto, S.; Greenbaum, S. G.; Grey, C. P. High Field Multinuclear NMR Investigation of the SEI Layer in Lithium Rechargeable Batteries. *Electrochem. Solid-State Lett.* **2005**, *8* (3), A145−A148.

(13) Gan, Z.; Gor'kov, P. L.; Brey, W. W.; Sideris, P. J.; Grey, C. P. Enhancing MQMAS of Low-γ Nuclei by Using a High B1 Field Balanced Probe Circuit. *J. Magn. Reson.* **2009**, *200* (1), 2−5.

(14) Ernst, H.; Freude, D.; Mildner, T.; Wolf, I. Laser-Supported High-Temperature MAS NMR for Time-Resolved in Situ Studies of Reaction Steps in Heterogeneous Catalysis. *Solid State Nucl. Magn. Reson.* **1996**, *6* (2), 147−156.

(15) Thurber, K. R.; Tycko, R. Measurement of Sample Temperatures under Magic-Angle Spinning from the Chemical Shift and Spin-Lattice Relaxation Rate of 79Br in KBr Powder. *J. Magn. Reson.* **2009**, *196* (1), 84−87.

(16) Chien, P.-H.; Feng, X.; Tang, M.; Rosenberg, J. T.; O'Neill, S.; Zheng, J.; Grant, S. C.; Hu, Y.-Y. Li Distribution Heterogeneity in Solid Electrolyte $Li_{10}GeP_2S_{12}$ upon Electrochemical Cycling Probed by ^7Li MRI. *J. Phys. Chem. Lett.* **2018**, *9* (8), 1990−1998.

(17) Wan, H. L.; Mwizerwa, J. P.; Han, F. D.; Weng, W.; Yang, J.; Wang, C. S.; Yao, X. Y. Grain-boundary-resistance-less $Na_3SbS_{4-x}Se_x$ solid electrolytes for all-solid state sodium batteries. *Nano Energy* **2019**, *66*, 104109.

(18) Hayashi, A.; Masuzawa, N.; Yubuchi, S.; Tsuji, F.; Hotehama, C.; Sakuda, A.; Tatsumisago, M. A sodium-ion sulfide solid electrolyte with unprecedented conductivity at room temperature. *Nat. Commun.* **2019**, *10*, 5266.

(19) Han, F.; Westover, A. S.; Yue, J.; Fan, X.; Wang, F.; Chi, M.; Leonard, D. N.; Dudney, N. J.; Wang, H.; Wang, C. High Electronic Conductivity as the Origin of Lithium Dendrite Formation within Solid Electrolytes. *Nat. Energy* **2019**, *4* (3), 187−196.

(20) Kuhn, A.; Kunze, M.; Sreeraj, P.; Wiemhöfer, H.-D.; Thangadurai, V.; Wilkening, M.; Heitjans, P. NMR Relaxometry as a Versatile Tool to Study Li Ion Dynamics in Potential Battery Materials. *Solid State Nucl. Magn. Reson.* **2012**, *42*, 2−8.

(21) Famprikis, T.; Canepa, P.; Dawson, J. A.; Islam, M. S.; Masquelier, C. Fundamentals of Inorganic Solid-State Electrolytes for Batteries. *Nat. Mater.* **2019**, *18* (12), 1278−1291.

(22) Zhang, Z.; Ramos, E.; Lalère, F.; Assoud, A.; Kaup, K.; Hartman, P.; Nazar, L. F. $Na_{11}Sn_2PS_{12}$: A New Solid State Sodium Superionic Conductor. *Energy Environ. Sci.* **2018**, *11* (1), 87−93.

(23) Bloembergen, N.; Purcell, E. M.; Pound, R. V. Relaxation Effects in Nuclear Magnetic Resonance Absorption. *Phys. Rev.* **1948**, *73* (7), 679−712.

(24) Prutsch, D.; Gadermaier, B.; Brandstätter, H.; Pregartner, V.; Stanje, B.; Wohlmuth, D.; Epp, V.; Rettenwander, D.; Hanzu, I.; Wilkening, H. M. R. Nuclear Spin Relaxation in Nanocrystalline β-Li_3PS_4 Reveals Low-Dimensional Li Diffusion in an Isotropic Matrix. *Chem. Mater.* **2018**, *30* (21), 7575−7586.

(25) Hanghofer, I.; Brinek, M.; Eisbacher, S. L.; Bitschnau, B.; Volck, M.; Hennige, V.; Hanzu, I.; Rettenwander, D.; Wilkening, H. M. R. Substitutional Disorder: Structure and Ion Dynamics of the Argyrodites Li_6PS_5Cl, Li_6PS_5Br and Li_6PS_5I. *Phys. Chem. Chem. Phys.* **2019**, *21* (16), 8489−8507.

(26) Wilkening, M.; Heitjans, P. From Micro to Macro: Access to Long-Range Li^+ Diffusion Parameters in Solids via Microscopic [6, 7]Li Spin-Alignment Echo NMR Spectroscopy. *ChemPhysChem* **2012**, *13* (1), 53−65.

(27) Meyer, M.; Maass, P.; Bunde, A. Spin-Lattice Relaxation: Non-Bloembergen-Purcell-Pound Behavior by Structural Disorder and Coulomb Interactions. *Phys. Rev. Lett.* **1993**, *71* (4), 573−576.

(28) de Klerk, N. J. J.; van der Maas, E.; Wagemaker, M. Analysis of Diffusion in Solid-State Electrolytes through MD Simulations, Improvement of the Li-Ion Conductivity in β-Li_3PS_4 as an Example. *ACS Appl. Energy Mater.* **2018**, *1* (7), 3230−3242.

(29) Hanghofer, I.; Gadermaier, B.; Wilkening, H. M. R. Fast Rotational Dynamics in Argyrodite-Type Li_6PS_5X (X: Cl, Br, I) as Seen by [31]P Nuclear Magnetic Relaxation—On Cation−Anion Coupled Transport in Thiophosphates. *Chem. Mater.* **2019**, *31* (12), 4591−4597.

(30) Neuberger, S.; Culver, S. P.; Eckert, H.; Zeier, W. G.; Schmedt auf der Günne, J. Refinement of the Crystal Structure of $Li_4P_2S_6$ Using NMR Crystallography. *Dalton Trans.* **2018**, *47* (33), 11691−11695.